Protein Engineering, Design and Selection, 2019, vol. 32 no. 10, pp. 443–457
doi: 10.1093/protein/gzaa008
Advance Access Publication Date: 13 May 2020
Original Article

Original Article

Exposure of a cryptic Hsp70 binding site determines the cytotoxicity of the ALS-associated SOD1-mutant A4V

Filip Claes[1,2,†], Stanislav Rudyak[1,2,3,†], Angela S. Laird[4,5], Nikolaos Louros[1,2], Jacinte Beerten[1,6], Maja Debulpaep[1,6], Emiel Michiels[1,2], Rob van der Kant [1,2], Joost Van Durme[1,2,6], Greet De Baets[1,2,6], Bert Houben[1,2], Meine Ramakers[1,2], Kristy Yuan[5], Serene S. L. Gwee[5], Sara Hernandez[4], Kerensa Broersen[1,6], Mikael Oliveberg[7], Barbara Moahamed[8], Janine Kirstein[8], Wim Robberecht[4], Frederic Rousseau[1,2,*], and Joost Schymkowitz[1,2,*]

[1]VIB Center for Brain & Disease Research, Switch Laboratory, Herestraat 49, Leuven, Belgium, [2]KU Leuven, Department of Cellular and Molecular Medicine, Switch Laboratory, Herestraat 49, Leuven, Belgium, [3]Emanuel Institute of Biochemical Physics, Russian Academy of Sciences, Leninskiy Prospekt, 14, Moscow 119991, Russia, [4]VIB, Center for Brain and Disease Research, Laboratory of Neurobiology, Herestraat 49, Leuven, Belgium, [5]Center for Motor Neuron Disease Research, Department of Biomedical Science, Faculty of Medicine, Macquarie University, Balaclava Rd, Macquarie Park, Sydney NSW 2109, Australia, [6]Applied Stem Cell Technologies, University of Twente, Technical Medical Centre, Drienerlolaan 5, Enschede, The Netherlands, [7]Stockholm University, Department of Biochemistry and Biophysics, Frescativägen, 114 19 Stockholm, Sweden, and [8]Universität Bremen, Fachbereich 2 Biologie/ Chemie, Postfach 330 440, Bremen, Germany

*To whom correspondence should be addressed. E-mails: Frederic.Rousseau@kuleuven.vib.be; Joost.Schymkowitz@kuleuven.vib.be

[†]These authors contributed equally to this work

Received 26 March 2020; Editorial Decision 31 March 2020; Accepted 21 April 2020

Abstract

The accumulation of toxic protein aggregates is thought to play a key role in a range of degenerative pathologies, but it remains unclear why aggregation of polypeptides into non-native assemblies is toxic and why cellular clearance pathways offer ineffective protection. We here study the A4V mutant of SOD1, which forms toxic aggregates in motor neurons of patients with familial amyotrophic lateral sclerosis (ALS). A comparison of the location of aggregation prone regions (APRs) and Hsp70 binding sites in the denatured state of SOD1 reveals that ALS-associated mutations promote exposure of the APRs more than the strongest Hsc/Hsp70 binding site that we could detect. Mutations designed to increase the exposure of this Hsp70 interaction site in the denatured state promote aggregation but also display an increased interaction with Hsp70 chaperones. Depending on the cell type, *in vitro* this resulted in cellular inclusion body formation or increased clearance, accompanied with a suppression of cytotoxicity. The latter was also observed in a zebrafish model *in vivo*. Our results suggest that the uncontrolled accumulation of toxic $SOD1^{A4V}$ aggregates results from insufficient detection by the cellular surveillance network.

Key words: ALS, cytotoxicity, HSP70, SOD1

Introduction

Accumulation and aggregation of misfolded proteins both inside and outside of neurons are associated to several neurodegenerative disorders, including Parkinson's, Alzheimer's and Huntington's diseases and amyotrophic lateral sclerosis (ALS) (Dobson, 2006). Each of these disorders is characterised by the accumulation of one or only a few specific proteins, the presence of which constitutes a pathological hallmark. Examples include the accumulation of Aß in Alzheimer's, α-synuclein in Parkinson's and huntingtin in Huntington's disease. Besides being disease markers, the misfolding and aggregation of these proteins is now widely viewed as participating if not being causative in the development of these diseases (Hardy and Selkoe, 2002; Polymenidou and Cleveland, 2011), as it seems these misfolded endogenous proteins acquire neurotoxic properties that are independent of wild type function (Winklhofer *et al*., 2008). Despite these observations, for most of these disorders it has remained difficult to relate disease progression and protein deposition (Perrin *et al*., 2009; Walker and LeVine, 2012).

It has become gradually apparent that observable protein deposits are probably not the most toxic fraction and that in fact the formation of misfolded protein inclusions might in some cases even be less toxic and part of a protective cellular response (Ciechanover and Kwon, 2015; Cohen *et al*., 2006). Neurotoxicity seems to originate from soluble misfolded protein oligomers (Bucciantini *et al*., 2002; Campioni *et al*., 2010). The mechanisms by which these soluble oligomers exert their toxic activity remains to be clarified (Benilova *et al*., 2012; Fandrich, 2012); however misfolded proteins are likely to interact with other cellular components including cellular membranes, other proteins and nucleic acids (Balch *et al*., 2008; Bence *et al*., 2001; Chiti and Dobson, 2006; Gidalevitz *et al*., 2006; Xu *et al*., 2011). The lack of correlation between visible protein aggregation and cytotoxicity has also been illustrated in a genetic screen for proteostatic modulators in *C. elegans*. Morimoto and colleagues found a number of genetic modulators that when silenced alleviated aggregation of polyQ and mutant SOD1 in muscle cells, but interestingly suppression of visible aggregation did not necessarily imply suppression of toxicity (Silva *et al*., 2011).

Motor neuron disease, also known as ALS, is an incurable, adult onset neurodegenerative disease characterised by muscle wasting and paralysis (reviewed in Boillee *et al*., 2006; Wijesekera and Leigh, 2009). The pathogenesis of sporadic ALS is not fully understood but involves the formation of inclusions of the RNA-binding protein TDP43 in motor neurons (Mackenzie *et al*., 2010). In 10% of patients the disease is inherited, associated to mutations in about 20 genes (Andersen and Al-Chalabi, 2011). Whereas *C9orf72* hexanucleotide repeat expansions, together with mutations in TDP43 and FUS appear to be the most common genetic cause of ALS (Andersen and Al-Chalabi, 2011; Wood, 2011), mutations in the gene encoding Cu/Zn superoxide dismutase (SOD1) are found in 20% of families with ALS (Khare *et al*., 2005). Wild-type SOD1 catalyses the conversion of superoxides into hydrogen peroxide, a reaction which requires the binding of Cu^{2+} and Zn^{2+}. Results from animal studies suggest that ALS is not caused by loss of normal SOD1 activity because deletion of wild-type SOD1 does not induce ALS (Polymenidou and Cleveland, 2011). Overexpression of mutant SOD1 in contrast, results in motor neuron degeneration, muscle denervation and weakness, and death (Dal Canto, 1995; Nagai *et al*., 2001; Ramesh *et al*., 2010; Wang *et al*., 2009). Therefore, a gain of toxic function has been suggested for mutant SOD1. The observation of SOD1 protein inclusions in motor neurons of mutant SOD1 ALS patients led to the proposal that in ALS, like in other neurodegenerative diseases, protein aggregation is a major player in the newly acquired toxic function of mutant SOD1 (Taylor *et al*., 2016). *In vitro*, however, wild-type and mutant SOD1 display only relatively mild aggregation propensities and mechanical agitation is needed to convert the protein from its native globular fold into amyloid-like aggregates (Chattopadhyay *et al*., 2008). Analysis of the SOD1 apo-protein showed further that most ALS mutations predominantly increase the unfolded form of SOD1 (Vassall *et al*., 2011), consistent with the observation that the globally unfolded state is the precursor for SOD1 fibrillation *in vitro* (Lang *et al*., 2012). Finally, non-native soluble SOD1 oligomers have been linked to cytotoxicity *in vitro* (Brotherton *et al*., 2013; Proctor *et al*., 2016; Redler *et al*., 2014; Sangwan *et al*., 2017) and soluble misfolded and oligomeric mutant SOD1 are detected throughout the life of ALS mouse models (Guo *et al*., 2010; Zetterstrom *et al*., 2007), suggesting that just like in other neurodegenerative diseases, SOD1 deposits themselves are not the major determinants of mutant SOD1 motor neuron toxicity.

Although mutant SOD1 inclusions stain positive for the molecular chaperones Hsp70 (Watanabe *et al*., 2001) and Hsp27 (Vleminckx *et al*., 2002), their individual overexpression does not confer a cytoprotective effect on cells containing SOD1 aggregates (Krishnan *et al*., 2006; Liu *et al*., 2005). However, conditioning cells with a mild heat shock does protect from mutant SOD1 mediated toxicity (Lin *et al*., 2013). This points towards the need for additional chaperones for SOD1 detoxification as in contrast to single heat shock protein overexpression, heat shock triggers a complex induction of the expression of heat shock proteins via the activation of the Hsf1 transcription factor (Mendillo *et al*., 2012). Motor neurons have been shown to have a high threshold for Hsf1 activation (Batulan *et al*., 2003), which is unfortunate as Hsf1 activation in the absence of heat is cytoprotective to mutant SOD1 (Lin *et al*., 2013).

The aim of this work was to revisit the relationship between protein aggregation, chaperone interaction and cytotoxicity in mutant SOD1. More than 150 mutations have been reported in SOD1 (Abel *et al*., 2012), but for this work we focussed on A4V as the most commonly reported SOD1 mutation occurring in about 50% of familial ALS patients in the US (Rosen *et al*., 1994). We identified a key Hsp70 interaction site in the amino acid sequence of SOD1 that is buried inside the hydrophobic core of the protein. Given that A4V overexpression does not lead to a potent heat shock response, we hypothesised that the mutation promotes the formation of aggregates that cannot efficiently be detected by the chaperones because of a disconnect between the exposure of aggregation prone regions (APRs) and of chaperone recognition sites. Hence, we designed destabilising mutations in the A4V background that aimed to increase the exposure of a Hsp70 binding site that is normally buried in the native state. In line with our design, the variants show an increase in aggregation propensity, Hsp70 interaction and the expression of several Hsp70 proteins. This leads to the collection of these SOD1 variants in large cellular inclusions and their clearance from the cell, resulting in an effective suppression of their cytotoxicity, both in cultured cells and in developing neurons in zebrafish embryos.

Our results suggest that mutations can increase aggregation propensity in a manner that goes undetected by the protein quality control machinery because of a mismatch between the APRs and the chaperone binding sites.

Results

Mapping aggregation-prone segments in wild-type and mutant SOD1

Protein aggregation is determined by the self-assembly of short aggregation-prone segments within a protein sequence into intermolecular ß-structured assemblies (Fernandez-Escamilla *et al*., 2004; Ventura *et al*., 2004). This intrinsic aggregation propensity of a protein sequence is generally mitigated by the burial of these aggregation-prone segments in the hydrophobic core of the folded protein, precluding their solvent exposure and self-assembly (Calamai *et al*., 2005). Protein aggregation can therefore be triggered by protein unfolding due to physiological stress or structurally destabilising mutations that expose these aggregation prone sequences. If these mutations also happen to occur within an aggregation-prone segments of the sequence, resulting in the increase of its intrinsic aggregation propensity, aggregation will be further promoted by an increased 'stickiness' of the protein sequence (Siekierska *et al*., 2012). There have been >150 mutations reported in SOD1 in ALS patients. To analyse the changes in the intrinsic aggregation propensity induced by these mutations, we employed the Waltz and Tango algorithms, which specifically predict amyloid and ß-sheet aggregation propensity, respectively (Fernandez-Escamilla *et al*., 2004; Maurer-Stroh *et al*., 2010; Rousseau *et al*., 2008). The results show that the overwhelming majority of these mutations do not increase the intrinsic aggregation propensity of the SOD1 sequence (Fig. 1A). This includes the frequently occurring and well-characterised mutant A4V, which we employ here as a representative disease mutation. We then proceeded to model all ALS-associated mutations on the atomic structure of SOD1 using the FoldX force field (Schymkowitz *et al*., 2005) in order to predict the effect of the mutations on the thermodynamic stability of the protein, calculated as $\Delta\Delta G$ in kcal.mol^{-1}. The histogram of these values (Fig. 1B) shows a large reduction of the thermodynamic stability of the protein for the majority of these mutants. The A4V mutant showed intermediate destabilisation compared to the majority of the mutations, but 2 kcal/mol is still a major destabilisation (Fig. 1B). For comparison, we show a similar histogram of >1300 validated single nucleotide polymorphisms from the SwissProt database (Boeckmann *et al*., 2003), which reveals a roughly bell-shaped curve centred around zero (described earlier, Siekierska et al., 2012; inset in Fig. 1B). Taking a closer look at the intrinsic aggregation propensity of the SOD1 sequence (Fig. 1C) reveals multiple APRs in the SOD1 sequence, which is largely consistent with what was found by others (Ivanova *et al*., 2014; Sangwan et al., 2017), and strongly suggests a complex aggregation mechanism, much like what was recently proposed for p53 (Wang and Fersht, 2017). Although our methods do not predict the 28–38 region identified by Sangwan *et al*., this peptide adds further complexity since it was shown that this region is important for the toxicity of aggregated SOD1. In the folded structure, the aggregating regions are all fairly close to the dimer interface of SOD1 (Fig. 1D). When peptides from these regions are incubated in phosphate-buffered saline (PBS) at room temperature, amyloid fibrils form spontaneously, as can be observed from the negatively stained transmission electron micrographs (Fig. 1E).

It is generally assumed that molecular chaperones of the Hsp70 family recognise misfolded proteins by binding to hydrophobic regions that are exposed in the misfolded state, but that are buried inside the native protein. Given the multiple APRs detected in the SOD1 sequence, we wondered if the Hsp70 binding sites perfectly overlapped with the aggregation driving regions. To this end, we used the method originally developed by Bukau and co-workers and which consists of measuring the binding of chaperones from the Hsp70 family to arrays of immobilised peptides (Rudiger *et al*., 1997). In the current study, we used a sliding seven amino acid window array over the SOD1 sequence in order to cover the entire polypeptide. The array was probed with recombinant human Hsp70 (HSPA1) and Hsc70 (HSPA8) and quantified for the amount of chaperone bound to each peptide. This approach revealed two central sequence stretches with clear Hsp70 and Hsc70 binding affinity (H_{63}FNPLSR$_{69}$ and I_{113}GRTLVV$_{119}$; Fig. 2A). To quantify the binding interactions, we performed microscale thermophoresis (MST) analysis, using labelled Hsc70 with a lysine-reactive fluorophore and both peptides as titrants (Supplementary Figure S1A). MST measurements reveal that I_{113}GRTLVV$_{119}$ is a strong binder, with a binding affinity (K_D = 7.1 µM) comparable to known Hsc70/Hsp70 interactors, such as FYQLALT (Swain *et al*., 2006; Takeda and McKay, 1996). On the other hand, the H_{63}FNPLSR$_{69}$ peptide shows a significantly lower affinity to Hsc70, similar to low affinities reported for other Hsc70 peptide binders, as for example the NR peptide substrate (NRLLLTG) (Swain et al., 2006; Takenaka *et al*., 1995). Comparison of the location of the APRs and Hsp binding sites (Fig. 1D) suggests that Hsp70 recognition and aggregation nucleation occur at distinct sites in the unfolded state of SOD1, which raises the question if the aggregation prone misfolded states of SOD1 that are populated by ALS-associated mutations also expose the Hsp70 recognition sites and can hence be cleared or whether there is a differential in exposure of both types of regions. Mapping of these regions onto the structure of SOD1 shows that the H_{63}FNPLSR$_{69}$ Hsp binding site (labelled as Hsp70A in Fig. 1D) is largely exposed in the native structure while I_{113}GRTLVV$_{119}$ binding site (labelled as Hsp70B in Fig. 1D) is completely buried. Moreover, when we used FoldX to calculate the predicted impact of disease-associated mutations on the local stability of the different residues in SOD1 (called $\Delta G_{contrib}$, as previously described, van der Kant *et al*., 2017), we found that this buried I_{113}GRTLVV$_{119}$ Hsp70-binding site is among the least affected regions, suggesting its local native structure is partly retained in mutant-induced misfolded states (Fig. 2B).

Modulating Hsp70 targeting to SOD1 A4V by rational design

In order to study the interplay between aggregation and Hsp70 recognition on the behaviour of mutant SOD1 in cells, we designed several mutations on the background of the prevalent A4V mutation. First, we introduced a proline residue in the strongest amyloid-forming region predicted by Waltz, i.e. APR1, via the N19P mutation. This mutation would be expected to show a reduction in the aggregation propensity or kinetics due to its ß-structure breaking properties but is not expected to affect Hsp70 binding as it does not affect the stability of the structure around the Hsp70 binding region (also, since the mutation leaves several other APRs in place, the aggregation propensity is by no means fully suppressed). Second, we aimed to destabilise the buried I_{113}GRTLVV$_{119}$ Hsp70 binding site. Therefore, we introduced tryptophan residues at several positions near or at the edges of the binding region via the G114W, V119W and G150W mutations (Fig. 2C). These mutations replace a small residue (Gly or Val) by the largest amino acid (Trp), which does not fit into the available space, giving rise to large steric clashes, either within the monomeric subunit, or between subunits in the dimer (Fig. 2C). Unsurprisingly, these mutations are predicted by FoldX to be highly destabilising with predicted $\Delta\Delta G$ values of

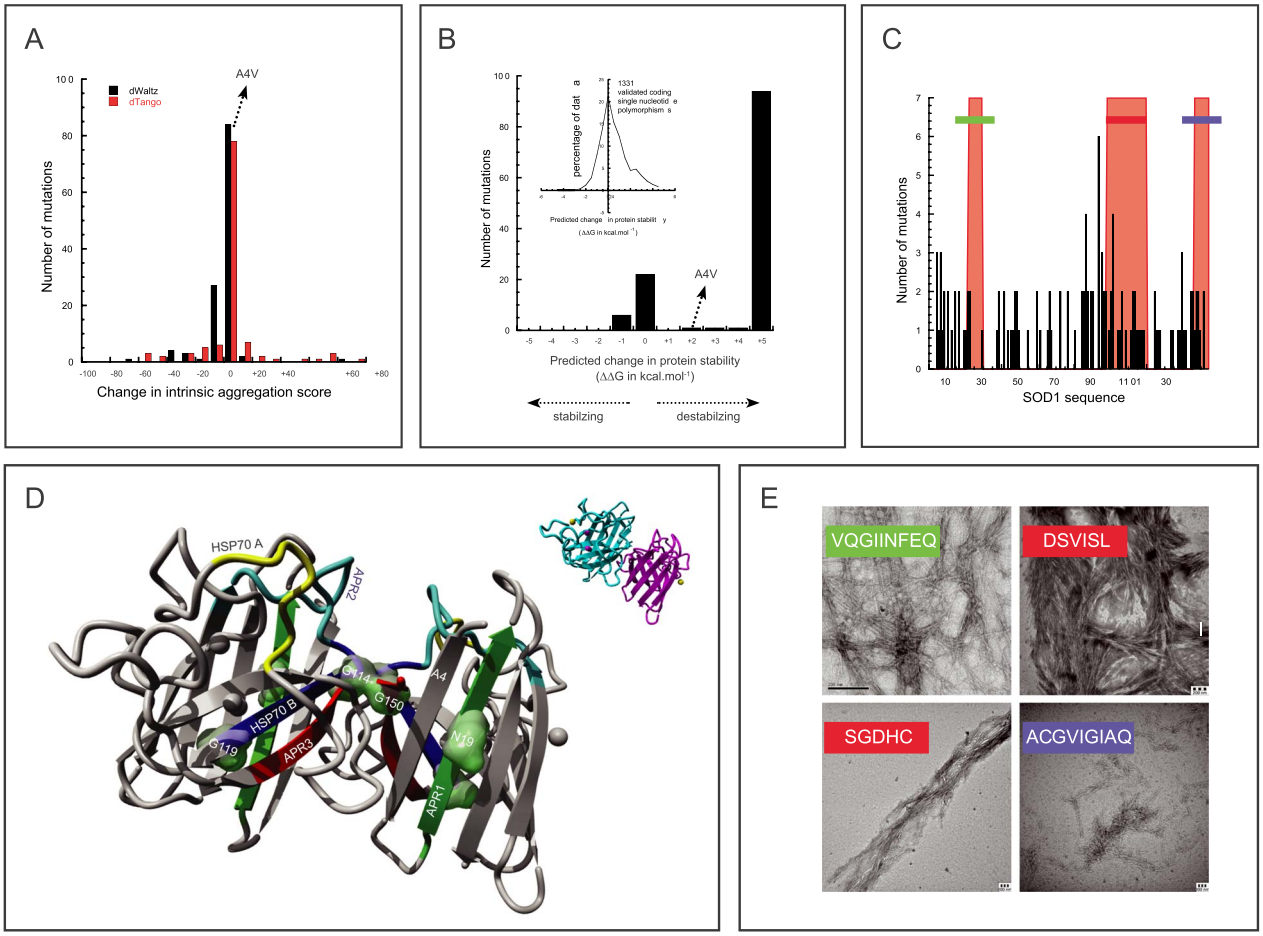

Fig. 1 Bioinformatic analysis of the aggregation propensity of wild-type and mutant SOD1. (**A**) Histogram of the change predicted by the general aggregation prediction algorithm TANGO (Fernandez-Escamilla *et al*., 2004) and the amyloid prediction algorithm Waltz (Maurer-Stroh *et al*., 2010) in the intrinsic aggregation propensity of SOD1 for all disease-associated mutations in the Database of Human Gene Mutation (>140 cases). (**B**) Histogram of the change predicted by FoldX in the thermodynamic stability of the SOD1 structure for the same mutants. The inset shows a similar histogram calculated for 1331 validated polymorphisms occurring in 577 proteins. (**C**) Plot of the number of mutations recorded per position along the SOD1 amino acid sequence (black bars). The three regions indicated in green, blue and red are predicted by the Waltz algorithm to have some propensity to form amyloid structure. (**D**) Schematic representation of the SOD1 structure (generated from pdb id 1 N19 using the Yasara software package). The regions indicated in colour correspond to the aggregation prone zones from C (APR1–3) and the Hsp70/Hsc70 binding sites. Residues mutated by rational design are also indicated. (**E**) TEM images of negatively stained amyloid fibrils grown from peptides corresponding to the APRs of SOD1. The colour codes correspond to the colour used in (C) and (D).

3.24 ± 0.10, 23.44 ± 3.72 and 5.47 ± 0.46 kcal/mol, respectively (very large ΔΔG values above 3–4 kcal/mol result from a strong penalisation of steric clashes by FoldX). These would hence be expected to lead to the increased exposure of any APRs or Hsp70 binding sites in that part of the sequence, due to decreased domain stability. We analysed the effect of these mutations on Hsp70 binding to the corresponding peptides in the chaperone binding assay described above and found that most mutations caused only a mild increase in Hsp70 binding (Supplementary Figure S1B), suggesting that although sequence intrinsic differences could play a role, the increased exposure of these regions is likely to constitute the major effect. To verify the aggregation propensity of our designed mutants, we recombinantly expressed the double mutants in *E. coli* and purified them from the soluble fraction (i.e. the supernatant after centrifugation, see methods) and analysed them immediately using size-exclusion chromatography coupled with multi-angle static light scattering (SEC-MALS, Fig. 2D), dynamic light scattering (DLS, Fig. 2E) and Thioflavin-T binding (ThT, Fig. 2F). In SEC-MALS, molecules are separated by size as in standard SEC, but the size of the eluting fraction is monitored using a multi-angle light scattering detector, which provides an absolute indication of mass. DLS provides an independent size estimation based on the diffusion coefficient of the sample and ThT is a dye that specifically binds to amyloid-like aggregates. All methods clearly show an increased aggregation of A4V compared to wild type, which is further exacerbated by the Trp mutations and reduced somewhat by the N19P mutation. The SEC-MALS shows the elution of large aggregate particles for the Trp double mutants, which was also independently observed in the DLS. This was accompanied by an increase in the ThT fluorescence, consistent with the formation of amyloid-like aggregates, likely due to increased exposure of APRs in the double mutants. However, transmission electron microscopy (TEM) analysis of the samples showed that the wild type aggregates we obtained, were only partially fibrillar in appearance and became even more amorphous for A4V and the double mutants (Supplementary Figure S1C). In fact, the aggregates have fractal appearance, consistent with diffusion-limited

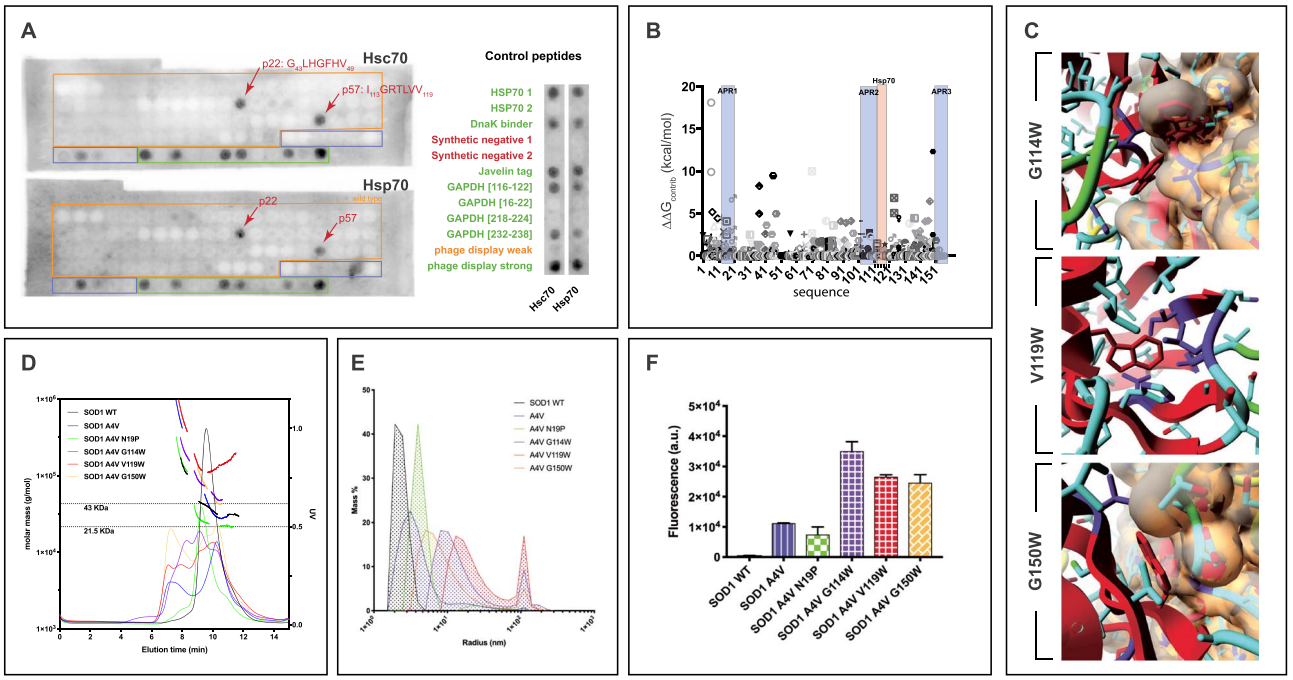

Fig. 2 SOD1 Hsp70/Hsc70 binding chracaterisation and mutant characterisation (**A**) Left panels show binding of Hsp70 and Hsc70 to an array of 74 overlapping 9-mer peptides systematically scanning the sequence of SOD1 by shifting the position of consecutive peptides by three residues. Hsp binding is detected via immuno-chemiluminescence (see methods) using the S-affinity tag fused to the Hsp protein. Right panels show a magnification of the control spots on both membranes, consisting of 3 weak or negative control peptides and seven positive control peptides derived from literature. Negative controls were two synthetic non-binding peptides and a weak binding peptide identified using phage display (Takenaka, Leung, McAndrew, Brown and Hightower, 1995, Van Durme *et al.*, 2009). The nine known Hsp/Hsc70 binding peptides were: (i and ii) VIAGLNVLRGS and PSYVAFTDTGS (Hsp 70 1 and 2) found using peptide arrays covering the Hsp70 sequence (Okochi *et al.*, 2008); (iii) NRLLLTGGS, (DnaK binder) the ligand in the solution structure of DnaK (Stevens *et al.*, 2003); (iv) NLLRLTGWGS the well-known 'Javelin' peptide ligand (Flechtner *et al.*, 2006); (v) FYQLALTGS discovered using phage display (Takenaka *et al.*, 1995). and (vi-ix) KRVIISAPGS, IHDNFGIVGS, FRVPTPNVGS and GKVIPELNGS found in a mass spectrometry study of Hsp70 binding sequences in GAPDH (Grossmann *et al.*, 2004). (**B**) The FoldX forcefield was used to calculate the predicted impact of disease-associated mutations on the local stability of the different residues ($\Delta\Delta G_{contrib}$) in SOD1. Locations of APRs are highlighted in blue, HSP70/Hsc70 binding site is highlighted in orange. (**C**) Structure zooms illustrating the large steric clashes introduced by the tryptophan mutants. These mutations replace a small residue (Gly or Val) by the largest amino acid (Trp), which does not fit into the available space, giving rise to clashes, either within the monomeric subunit (V119W), or between subunits in the dimer (G114W and G150W). (**D**) Light scattering data and measured molar mass of SOD1 variants following separation by size-exclusion chromatography. SOD1 wild type forms dimers, whereas the A4V mutation is slightly destabilising and the A4V/N19P double mutant keeps the protein primarily in a monomeric fraction. Promotion of aggregation is validated by the presence of species with larger molar masses for the A4V/G114W, A4V/119 W and A4V/150 W double variants. (**E**) Particle size distribution of SOD1 variants measured with DLS. SOD1 WT, A4V and A4V/N19P to a lesser extent, remain soluble, whereas particles with a large hydrodynamic radius are formed by the A4V/G114W, A4V/119 W and A4V/150 W double mutants. (**F**) Thioflavin-T (ThT) fluorescence, a measure for the formation of amyloid structure, shows that the three double mutants augment amyloid aggregation in the A4V background, while the proline mutant in the first APR lowers it.

aggregation, likely resulting from the multiple APRs in this protein, leading to fast aggregation and low order. These results corroborate our designs, but also show that increased destabilisation of this region of the protein leads to increased aggregation propensity, as well as the exposure of the cryptic Hsp70 binding site (see below).

Destabilising A4V induces inclusion formation

To study the behaviour of these SOD1 A4V variants in the cell, we transiently overexpressed full-length wild-type SOD1, as well as the disease mutation A4V and the double mutants A4V/N19P, A4V/G114W, A4V/V119W and A4V/G150W in HeLa cells, a non-neuronal cell line that is not sensitive to the toxic properties of the A4V SOD1 disease mutant (Supplementary Figure S2A) eliminating toxicity as a confounding factor in these assays. Analysis of the subcellular localisation of these SOD1 variants by fluorescence microscopy (Fig. 3A and Supplementary Figure S4) revealed a uniform diffuse cytoplasmic distribution for wild-type SOD1, as well as the A4V single and A4V/N19P double mutants. In contrast, the destabilising A4V/G114W, A4V/V119W and A4V/G150W double mutants showed the frequent formation of large perinuclear inclusions, albeit with poor contrast due to the persistence of a diffuse background. Quantification of the percent of cells showing these inclusions for the different SOD1 constructs confirmed the large difference in inclusion formation displayed by the A4V/G114W, A4V/V119W and A4V/G150W mutants (Supplementary Figure S2B).

To assess the nature of these protein inclusions biochemically, we first performed solubility fractionation experiments. To this end, HeLa cells transiently transfected with the different SOD1 variants were lysed in a mild solubilizing lysis buffer and the insoluble protein fraction was collected by centrifugation (13 000 g). The pelleted protein fractions were next solubilised in 8 M urea. This analysis showed that while wild-type SOD1 is almost completely soluble (pellet fraction < 10%, further called insoluble), the A4V disease mutant produces an insoluble fraction that reaches ~40% of total SOD1 protein (Fig. 3B). The introduction of the aggregation-lowering N19P mutation in the A4V background reduced the insoluble fraction

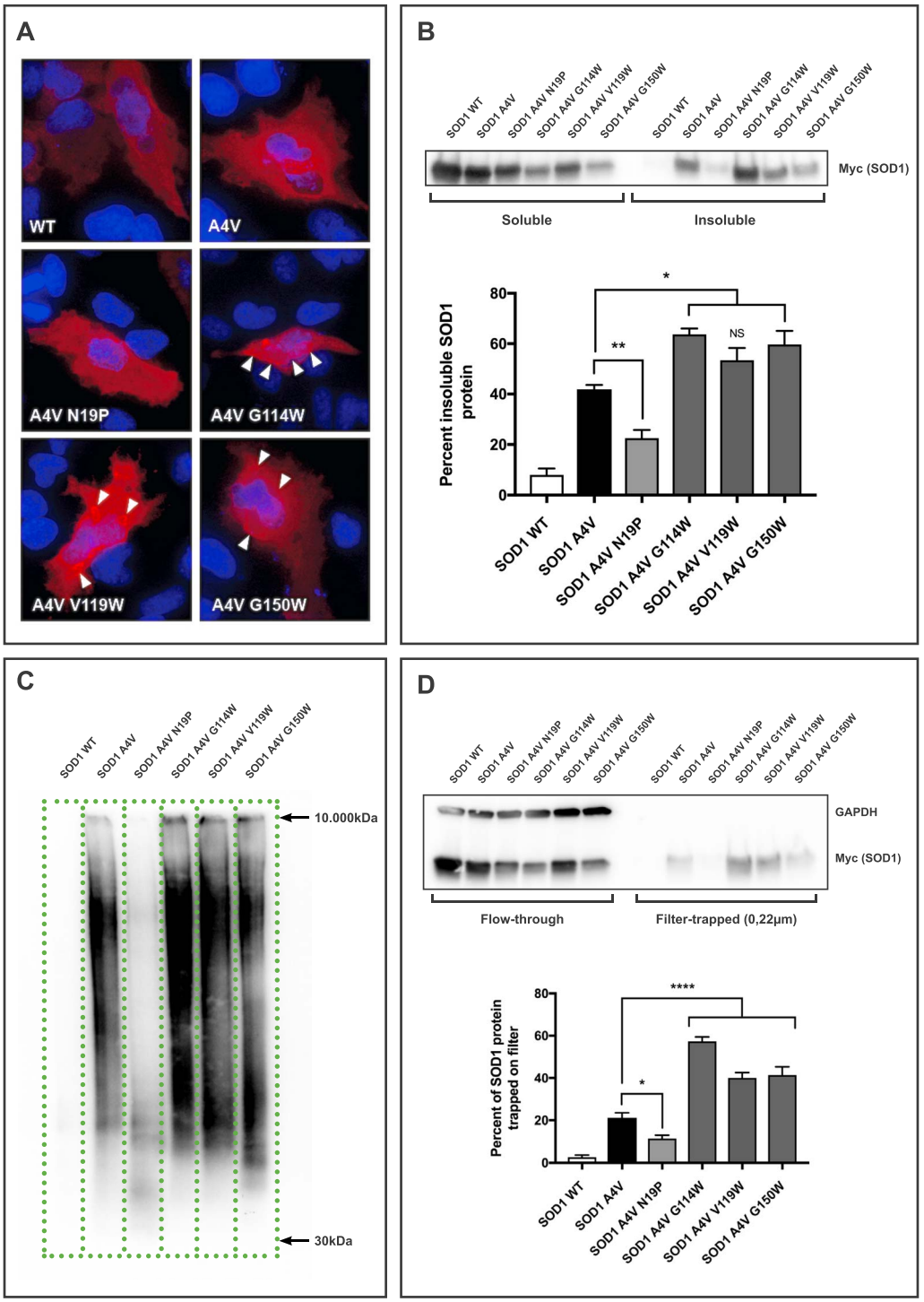

Fig. 3 Characterisation of aggregation behaviour *in cellulo*. (**A**) Representative immunofluorescent staining of HeLa cells expressing the different SOD1 variants (red). While SOD1 wild type, A4V and A4V/N19P show a diffuse staining pattern, the aggregation-promoting double mutants A4V/G114W, A4V/V119W and A4V/G150W show the formation of large perinuclear inclusion-like structures (white arrowheads). (**B**) Solubility fractionation of lysates from HeLa cells transiently overexpressing SOD1 wild type or mutants. Graph shows the quantification of the insoluble fraction for each SOD1 variant. While almost no insoluble fraction was detected for SOD1 wild type, around 40% of the total A4V disease mutant was detected in the insoluble fraction. Introducing the aggregation-blocking N19P mutation on the A4V background significantly reduced the insoluble fraction. Conversely, introducing the destabilising G114W, V119W or G150W mutations resulted in a larger insoluble fraction. Error bars represent the SEM, $^{*}P < 0.05$; $^{**}P < 0.01$. (**C**) BN-PAGE of total cell lysates from HeLa cells expressing the corresponding SOD1 variants. (**D**) Assessment of SOD1 aggregate size by the filter trap assay. Cell lysates from SOD1 transfected cells were filtered through 0.22 µm membranes and flow-through and trapped fractions were blotted and probed for GAPDH and SOD1. Quantification (lower graph) of these blots revealed that for the destabilising double mutants a significantly larger fraction was trapped on the filter as compared to the A4V single mutant. For the aggregation-reducing double mutant A4V/N19P, significantly less protein was trapped on the filter. Error bars represent the SEM, $^{*}P < 0{,}05$; $^{****}P < 0{,}001$.

again to ~20%; however, all three destabilising mutants increased the insoluble fraction to >50%. To further characterise the stability of the insoluble fraction formed by the different SOD1 variants, we performed serial solubility extractions. Proteins from HeLa cells transfected with a given SOD-1 variant were extracted in buffers of increasing denaturing strength. The following extraction buffers were used (refer to material and methods for formulations): (i) NP40 buffer, (ii) RIPA buffer, (3) RIPA with 2% SDS and finally (4) 8 M urea. The insoluble fraction in a given buffer is collected by centrifugation and resuspended in the next buffer in the series. The more stable aggregates are then expected to end up in the least soluble fractions. This therefore allows us to assess the differential in stability of aggregates formed by different mutants and shows that the A4V/G114W, A4V/V119W and A4V/G150W double mutants do form more stable aggregated fractions as compared to the single A4V mutant, as evidenced by an increase the fraction resistant to 2% SDS (Supplementary Figure S2C). Introduction of the N19P, however, destabilises the insoluble fraction.

To assess the size range of the aggregates formed by these different mutants, we first performed Blue Native PAGE (BN-PAGE) analysis. These data show that while wild-type SOD1 runs as a (hardly detectable) dimer, the A4V disease mutant forms a high molecular weight smear ranging from the monomer up to the upper size limit of the gel (10 000 kDa; Fig. 3C). The A4V/N19P double mutant, however, shows significantly less smearing, confirming the dominant role of the N-terminal aggregation-prone region as identified by the Waltz algorithm in the aggregation of the A4V disease mutant. The aggregation promoting mutants all show high molecular weight smears similar to the single A4V mutant, although there appears to be more protein that was impaired in entering of the native gel as compared to the A4V single mutant, indicating these double mutants formed larger sized aggregates. To confirm this observation more conclusively, we performed filter trapping experiments, in which whole cell lysates of cells expressing the different SOD1 variants were filtered through a 0.22 μm filter. Proteins trapped on the filter were next recovered by stringent washes. SOD1 levels in the flow through and trapped fractions were quantified using western blot. This analysis confirmed that the destabilising A4V/G114W, A4V/V119W and A4V/G150W double mutants indeed form larger aggregates as compared to the other mutants as evidenced by the larger fraction trapped on the filter (Fig. 3D).

Together, these analyses confirm *in cellulo* that by rational design we have modulated the stability and consequently aggregation behaviour of the A4V disease mutant.

Modulating the stability of A4V affects heat shock response

As inclusion formation is an active cellular defence mechanism initiated by proteostatic surveillance mechanisms, we next analysed the heat shock response upon expression of these mutants in HeLa cells. The distinction in protein behaviour between these mutations coincided with their effect on Hsp70, Hsp70B′ and Hsc70 protein levels as analysed by western blot (Fig. 4A). Heat shock protein levels were normalised to SOD1 expression levels to minimise interpretation errors due to differences in transfection efficiency and expression levels. While expression of A4V leads to only a minor increase in the detected Hsp levels, expression of the destabilising double mutants leads to clear increase in the level of Hsps. Moreover, the aggregation reducing mutation A4V/N19P to a large extent appears to exert a similar induction as the aggregation-promoting double mutants. These data suggest that while the small soluble aggregates formed by the A4V disease mutant escape proteostatic surveillance, the variants in which the I_{113}GRTLVV$_{119}$ Hsp binding site was destabilised are readily detected and therefore induce a robust proteostatic response. The latter appears to be confirmed by solubility fractionation (as described above) for Hsp70 and Hsp70B′ as these chaperones show a similar solubility profile as the corresponding SOD1 mutant expressed in the cell (Fig. 4A and Supplementary Figure S3A). Similarly, probing the protein fractions generated by filter-trapping (see above) for Hsp70 and Hsp70B′ showed a comparable enrichment of these Hsps on the filter for the aggregation-promoting double mutants (Supplementary Figure S3B).

To probe this further, we performed co-immunoprecipitation experiments to assess whether Hsp70 and Hsp70B′ and the different SOD1 mutants reside in the same complex. Comparison of the normalised levels of immunoprecipitated Hsp70 and Hsp70B′ to SOD1 between the A4V disease mutant and all of the double mutant showed that several of the aggregation-promoting double mutants were significantly more promiscuous in complexing Hsp70 and Hsp70B′ (Fig. 4B). Interestingly, while the aggregation-reducing double mutant A4V/N19P was able to induce a heat shock response, as shown above, it failed to efficiently precipitate Hsps, suggesting that this induction is an indirect effect independent from direct Hsp engagement. These observations were furthermore confirmed by immunofluorescent analysis of HeLa cells expressing the different SOD1 variants for Hsp70, which shows an enrichment of Hsp70 in the protein inclusions formed by the aggregation-promoting double mutants (Supplementary Figure S4). Although none of these measurements unequivocally demonstrate a direct interaction with the chaperone, all the data together strongly suggest this as a most likely scenario.

Modulating the stability of A4V affects degradation rates

To assess the consequences of the observed differences in heat shock response, we proceeded to compare the degradation rates of our mutants in the soluble and insoluble protein fractions by ribosomal inhibition through cycloheximide treatment (Fig. 5A). These data show that wild-type SOD1 is a relatively long-lived protein, whose levels show no decrease during the 9 h observation period used in this experiment. The A4V mutant is less stable and degraded at a faster rate in the soluble fraction (~30% reduction after 9 h) while the insoluble fraction stays constant during the observation period. However, the double mutations strongly alter the degradation rates: both the less aggregating A4V/N19P mutant and the destabilising A4V/G114W, A4V/V119W and A4V/G150W mutants are degraded significantly more rapid in the soluble fraction (levels reduced by > 65% after 9 h), whereas again no significant differences could be observed in the insoluble fractions over the observation period. These results show that soluble oligomeric aggregates like those formed by the A4V mutant slow down the degradation of misfolded proteins, but that aggresome formation such as in A4V/G114W, A4V/V119W and A4V/G150W speeds up degradation, consistent with the notion that aggresomes are formed at the centres of protein degradation in the cell. Moreover, an equally effective route to enhance clearance of the misfolded protein is to neutralise the APR driving A4V aggregation, such as in A4V/N19P.

To test whether these observed differences in degradation in HeLa cells also hold true in a more relevant cell type, we resorted to the NSC-34 motor neuron cell line, a hybrid cell line between mouse

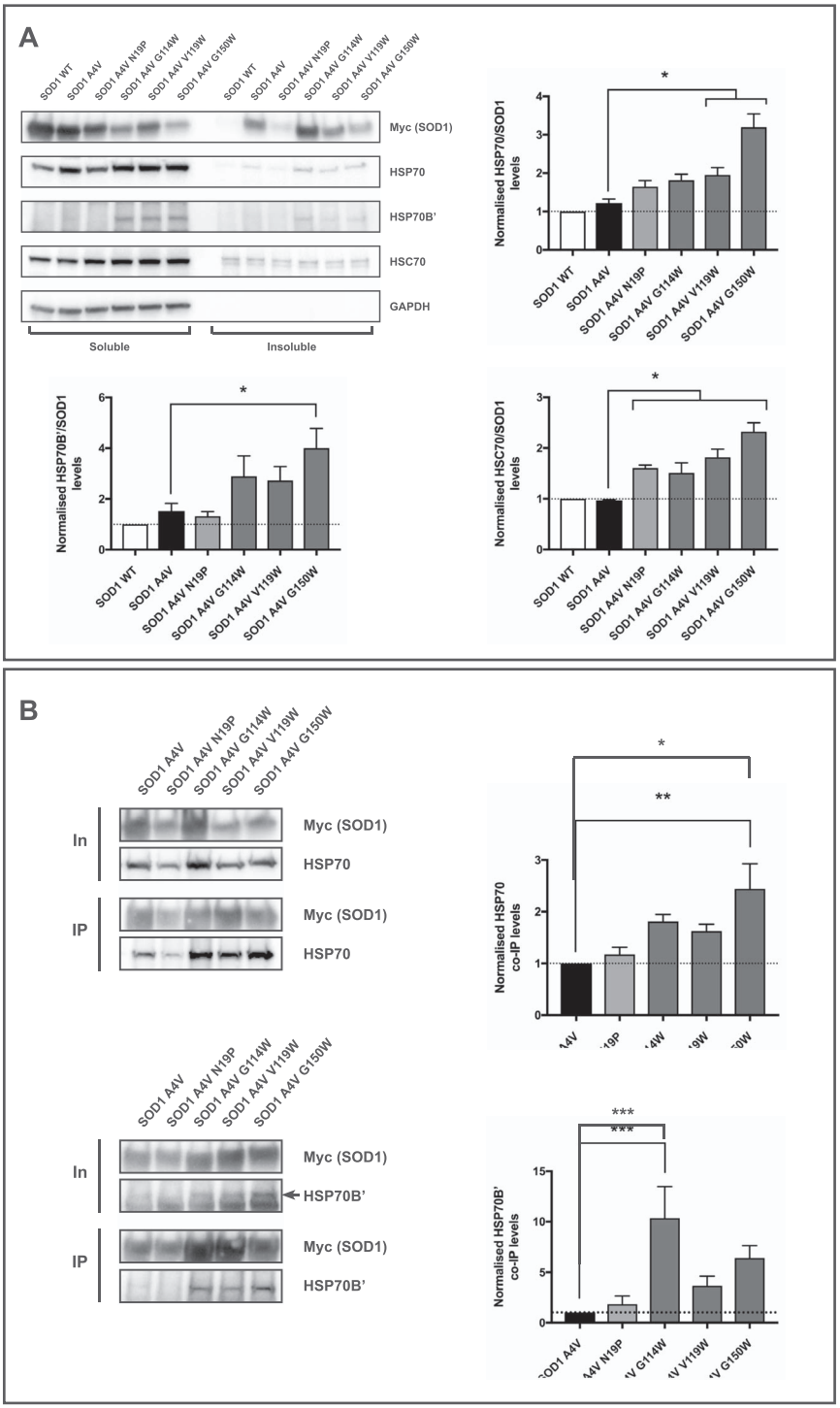

Fig. 4 Heat shock response in HeLa cells overexpressing SOD1. (**A**) Representative western blots of solubility fractionated cell lysates from HeLa cells transiently overexpressing the different SOD1 variants, probed Hsp70, Hsp70B′, Hsc70 and GAPDH. Graphs show quantification of the ratio of total (soluble + insoluble) protein levels for each Hsp to the corresponding SOD1 total protein level, normalised to the wild type condition. Error bars represent the SEM, $^{*}P < 0.05$. (**B**) Co-immunoprecipitation of each of the SOD1 variants with Hsp70 or Hsp70B′. Representative western blots of input and immunoprecipitated fractions are shown on the left, quantification of the ratio of immunoprecipitated Hsp to SOD1 normalised to the A4V condition are shown on the right. Error bars represent the SEM, $^{*}P < 0.05$, $^{***}P < 0.005$.

neuroblastoma cells and mouse spinal cord which is commonly used as a cellular model to investigate the physio-pathological mechanisms of ALS. Therefore, we first generated NSC-34 cells stably expressing either wild type, A4V, A4V/N19P, A4V/G114W, A4V/V119W or A4V/G150W SOD1. We next assessed protein levels by western blot and found that while wild-type SOD1 was readily detected in these cells, all mutant proteins were detected at significantly lower levels (Fig. 5B). Expression of the disease mutant

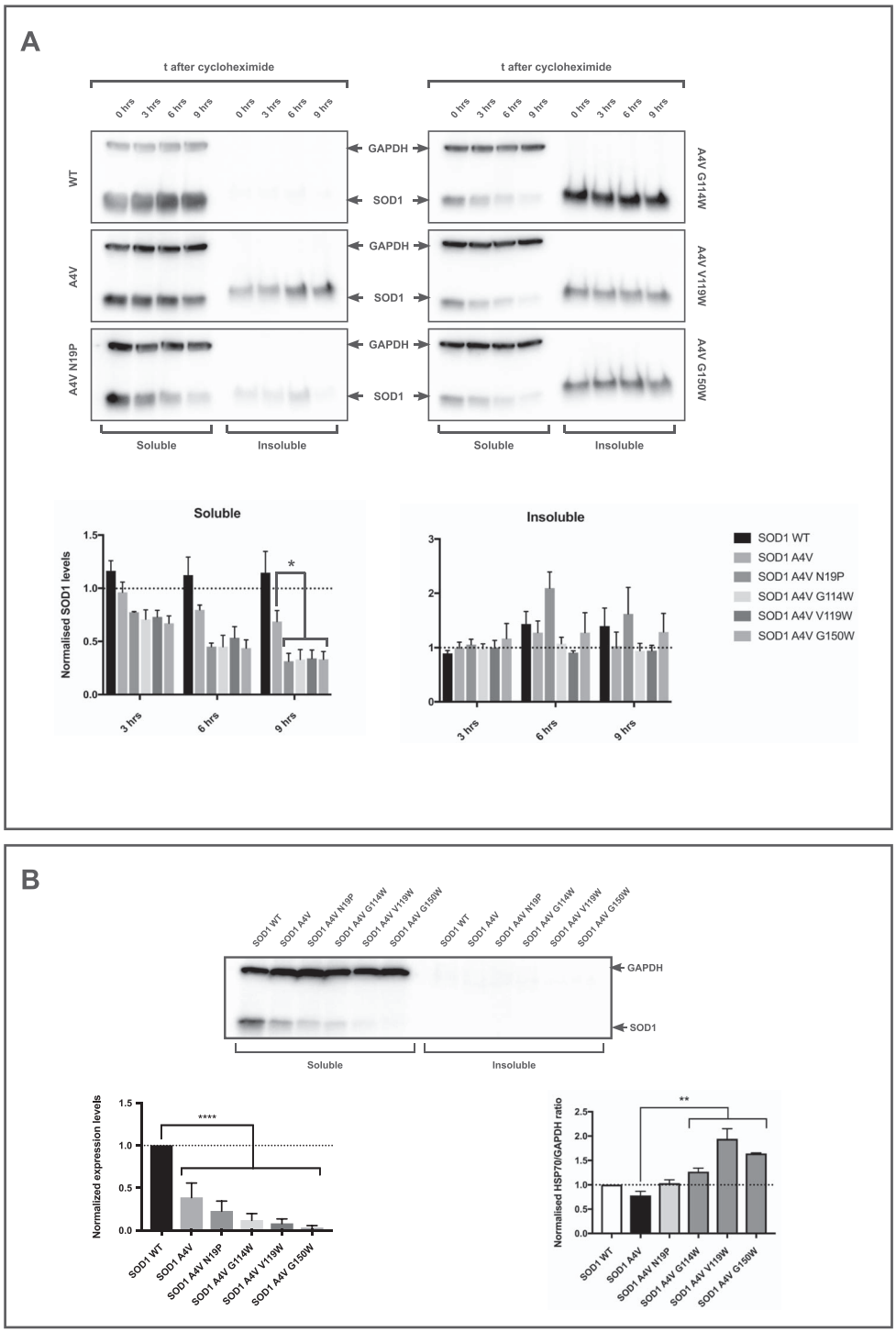

Fig. 5 Degradation of wild-type and mutant SOD1. (**A**) Cycloheximide chase experiments to assess degradation of wild-type and mutant SOD1. Twenty-four hours after transfection of HeLa cells with the indicated SOD1 variants, cells were treated with 40 μg/ml cycloheximide. At indicated time points after cycloheximide treatment, cells were lysed and soluble and insoluble fractions were generated and analysed by western blot for SOD1 (myc) and GAPDH. Representative western blots are shown in the top panels and densitometric quantifications of soluble and insoluble fractions are shown in the lower panels. (**B**) Fractionation of lysates from NSC-34 cells stably expressing the different SOD1 variants into soluble and insoluble fractions by centrifugation, analysed by western blot. Representative blot for SOD1 (myc) and GAPDH is shown in the top panel and quantification is shown in the lower left panel. Quantification of the Hsp70 levels normalised to GAPDH is shown in the lower right graph.

A4V was reduced by >60% as compared to wild type; however, expression of the double mutants was reduced even further with the aggregation-reducing double mutant A4V/N19P showing > 75% reduction and the aggregation-promoting double mutants showing > 85% reduction. To assess whether these differences are indeed caused by differences in degradation we studied protein levels after

inhibition of proteasomal and/or macroautophagic degradation. While single inhibition of either proteasomal degradation using Bortezomib or macroautophagic degradation using 3-methyladenine (3-MA) moderately increased the levels of mutant proteins, only combined inhibition restored mutant protein levels to or beyond the wild type level, except for the A4V/G150W double mutant, indicating that this mutant is degraded through an alternative pathway (Supplementary Figure S5). Interestingly, only inhibition of proteasomal degradation resulted in the appearance of an insoluble fraction for the aggregation-promoting double mutants (Supplementary Figure S5), suggesting that proteasomal degradation of soluble protein forms the first line of defence against the accumulation of aggregation-prone misfolded SOD1 proteins which leads to formation of an insoluble fraction. Consequently, inhibition of macroautophagy only does not increase the insoluble fraction.

Finally, western blot analysis of Hsp70 levels in these cell lines showed that, similarly to what was observed in HeLa cells, the expression of the aggregation-promoting double mutants resulted in a significant increase in Hsp70 protein levels as compared to the A4V single mutant (Fig. 5B).

Modulating the stability of A4V affects cytotoxicity readouts

To assess whether these findings affect the neuronal toxicity phenotype induced by mutant SOD1, we first assessed the toxicity induced by expression of these SOD1 variants in the stable NSC-34 cell lines. To this end, we assessed cell viability 24 h after plating equal number of cells for each stable line. As expected, expression of the A4V disease mutant resulted in a reduction of ∼30% in cell viability (Fig. 6A). However, while expression of both the aggregation-reducing double mutants A4V/N19P as well as the aggregation-promoting double mutants A4V/G114W, A4V/V119W and A4V/G150W appeared to alleviate this reduction in cell viability, this effect was significant for the A4V/V119W mutant only.

Next, we studied a well-established model for mutant SOD1 toxicity *in vivo*, the motor neuron axonopathy model in zebrafish overexpressing mutant SOD1 (Lemmens *et al*., 2007; Ramesh *et al*., 2010; Van Hoecke *et al*., 2012). We therefore expressed the corresponding zebrafish orthologues for the SOD1 variants we tested, i.e. wild type, A4V, A4V/N19P, A4V/G113W, A4V/V118W and A4V/G150W, by injecting mRNAs encoding these mutants in one to four cell-stage zebrafish embryos and evaluated the effect on motor neuron axonal length in the trunk of 30 h post-fertilisation (hpf) embryos (Fig. 6B). To this end, primary motor neurons were fluorescently labelled in fixed embryos and the length of the Caudal primary (CaP) motor neuron axons was measured. As previously reported (Lemmens *et al*., 2007), expression of SOD1 A4V resulted in a significant reduction of CaP axon length (Fig. 6C). The aggregation reducing mutation A4V/N19P induced an axonopathy similar to the A4V disease mutant, even though protein accumulation is less for similar mRNA levels injected (consistent with the observations in mammalian cells of increased degradation). However, introduction of a G113W or V118W mutation in A4V SOD1 partially rescued the observed axonopathy and also gave rise to a reduction in protein levels in the embryonic system, as was observed *in cellulo* (Fig. 6B and C). These results suggest that the formation of soluble aggregates, such as is observed for A4V is not a critical feature for motor neuron toxicity, since its abolition does not necessarily reduce the axonopathy readout. On the other hand, the destabilising double mutants with increased heat shock propensity A4V/G113W, A4V/V118W and A4V/G150W appear to supress motor neuron toxicity.

Taken together these data suggest that neurotoxicity of A4V mutant SOD1 is not solely defined by its ability to form soluble oligomers but rather stems from its ability to escape binding of heat shock proteins, resulting in the accumulation of toxic species in the cell. In fact, for some of the less toxic mutants, when the toxicity is normalised to the protein levels remaining in the cell, it becomes clear that the species may actually be more toxic to the cell per unit of protein, but they are rescued by the increased clearance they induce.

Discussion

The role of protein aggregation in protein misfolding diseases has been a matter of extensive debate. Whilst the presence of both intracellular and extracellular misfolded protein inclusions is a recognised pathological hallmark, it is difficult to find a clear correlation between protein deposition and disease progression. However, the association of specific misfolded proteins to distinct pathologies and the observation that misfolded proteins acquire cytotoxic properties suggest an active and specific role for protein aggregation in disease development. The inconsistency opposing aggregation as a disease marker to its weak diagnostic value may be resolved by evidence indicating that aggregate toxicity results from small soluble and highly diffusive oligomers, rather than from large protein inclusions (Bieschke *et al*., 2012), which are hallmarks of a cellular response to contain the aggregates within distinct subcellular compartments (Kaganovich *et al*., 2008).

Studying the relationship between protein aggregation and cytotoxicity is extremely challenging because aggregation is a highly heterogeneous kinetic phenomenon generally precluding the isolation of stable intermediates and in particular small soluble oligomers. Moreover, these soluble oligomers, which seem to be the most relevant species, are undetectable by standard microscopy techniques. In light of these limitations, a straightforward approach to study aggregation–toxicity relationships is comparing several disease mutants of a particular disease-associated protein. Here we examined SOD1, a protein in which >150 different disease-causing mutations have been identified (Abel *et al*., 2012). We first aimed to determine which segments of the SOD1 sequence have a tendency to self-assemble in ß-structured aggregates, thereby contributing to the intrinsic aggregation propensity or 'self-stickiness' of the sequence. In addition, we determined the regions of the SOD1 polypeptide chain that can be recognised by the molecular chaperones of the Hsp70 family. Strikingly, there is very little overlap between the regions that cause SOD1 aggregation and those that mediate Hsp70 interaction. As destabilising mutants increase the fraction of unfolded SOD1, these regions will become more frequently exposed and the aggregation propensity of the protein will increase. SOD1 mutations are scattered throughout 74 out of the 153 amino acid positions of the protein, destabilising different structural elements with varying magnitudes, resulting in mutants with differing unfolded and partially folded conformational distributions. These mutant-specific conformational distributions of misfolded SOD1 will likely result in differential exposure of one or several of the three aggregation prone segments, but this will not necessarily result in increased Hsp70 interaction through increased binding site exposure. This appears to be particularly true for the I_{113}GRTLVV$_{119}$ Hsp binding site since this region resides buried in a stable part of the SOD1 structure that appears to be little affected by the disease associated mutations.

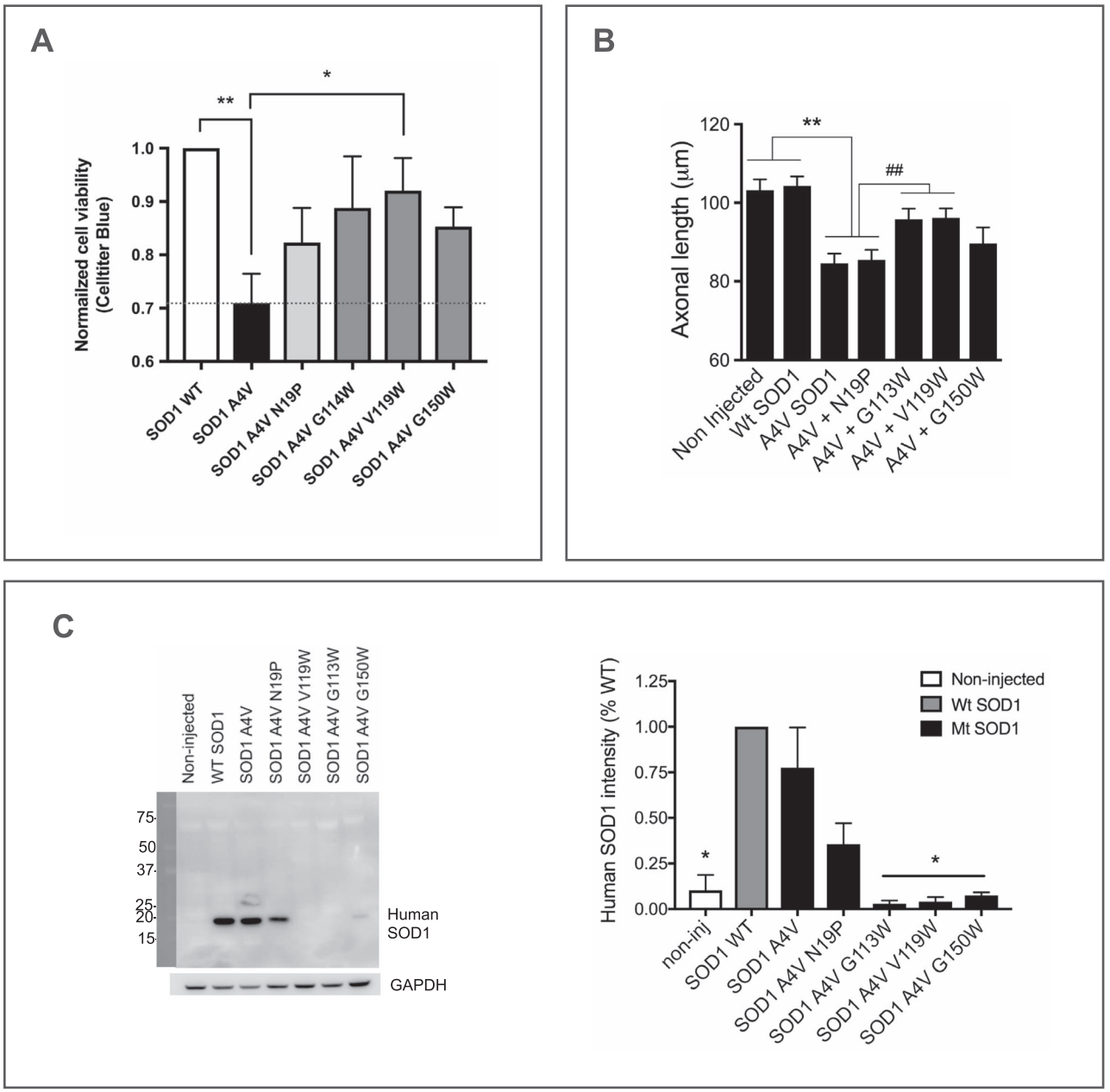

Fig. 6 Toxicity of wild-type and mutant SOD1 *in vitro* and *in vivo*. (**A**) Cell viability of NSC-34 cells stably expressing SOD1 variants as assessed by the CellTiter blue assay 24 h after plating. While expression of the A4V mutant reduces cell viability by ~30%, expression of both the aggregation-reducing double mutants A4V/N19P as well as the destabilising double mutants A4V/G114W, A4V/V119W and A4V/G150W alleviated this reduction in cell viability. (**B**) Overexpression of A4V mutant SOD1 mRNA resulted in motor axon pathology characterised by decreased axon lengths in zebrafish expressing A4V SOD1 as compared to non-injected or wild-type SOD1 expressing embryos. Zebrafish expressing the aggregation mitigating mutant (A4V/N19P) exhibited a similar degree of axonopathy to the A4V mutant, $^{**}P < 0.001$. However, zebrafish expressing the destabilised A4V variants (A4V/G113W and A4V/V119W) displayed significantly longer motor axons that those expressing the disease-causing A4V variant, $^{\#\#}P < 0.0001$. (**C**) Lysates from zebrafish expressing the different SOD1 variants were analysed by western blot for human SOD1. Representative blots for SOD1 and GAPDH are shown in the left panel and quantification is shown in the right panel. $^{*}P < 0.05$.

Using our understanding of the locations of the aggregation determining and Hsp70-binding sequence segments within SOD1 we designed variants of the A4V disease-associated mutation that aimed to decrease the aggregation propensity (N19P) or to increase the exposure of the $I_{113}GRTLVV_{119}$ Hsp70 binding site (G114W, V119W and G150W). As we are not able to monitor in sufficient detail the complex and sometimes subtle differences in conformational compositions of different SOD1 mutants we reasoned that we could still extract some knowledge on the relationship between aggregation, chaperone interaction and toxicity by drastically changing the Hsp70 affinity of a single disease mutant. We explored the toxic effects of these variants both *in vitro* and *in vivo* by examining the extent of cell death and of a motor axonopathy found in mutant SOD1 (e.g. A4V) expressing motor neuron-like NSC-34 cells and zebrafish embryos, respectively. We found that by increasing the exposure of the $I_{113}GRTLVV_{119}$ Hsp70 binding site in A4V did consistently alleviate the axonal toxicity of A4V SOD1. Thus, while A4V both forms aggregates and is neurotoxic, we were able to

construct variants of A4V that are toxic without aggregating and vice versa, variants that aggregate, but are not toxic. This ability to uncouple aggregation and toxicity indicates that mutant SOD1 toxicity is not strictly dependent on the intrinsic aggregation propensity of its sequence but, rather, that it is the cellular response to SOD1 misfolding that determines this toxicity.

Indeed, in both HeLa cells and NSC-34 cells, we found that overexpression of the variants of A4V that have an increase exposure of the Hsp70 binding site, show an induction of the expression of all Hsp70-family members assessed in this study. Although the Hsp70 expression profile appears to differ between these mutants, they all result in a strong increase in inclusion body formation and/or degradation of mutant SOD1, leading to a suppression of cytotoxicity. Our results suggest that, paradoxically, it is the inability of mutant SOD1, and possibly of other misfolding-associated proteins, to efficiently aggregate that is responsible for its toxicity. Finally, chaperone affinity might provide an explanation for the widespread toxicity that seems to be associated with small diffusible oligomers in different aggregation diseases. If heat shock response is dependent on chaperone affinity for aggregates then the differential exposure of chaperone binding sites and APRs in disease-associated mutations might cause these aggregates to escape the vigilance of the proteostatic surveillance system.

Last, but not least, the differences between the different mutants are quite subtle and complex and some of our results seem to differ slightly, depending on which mutant is considered. For example, the 150 W variant does not always show the same behaviour as the others in the assays used. Hence, there are likely subtle sequence effects that alter the precise folding and aggregation kinetics—chaperone binding—biological outcome. These considerations preclude drawing firm conclusions from our data, but all things considered, the data support a model where recognition by Hsp70 is separated in the primary sequence from aggregation propensity, so that mutations can trigger aggregation without leading to an appropriate chaperone response, as would be required for preventing the cytotoxicity of these aggregates (Supplementary Figure S6).

Materials and Methods

DNA constructs and manipulation

Coding DNA of SOD1 was amplified from human brain cDNA library (Invitrogen) and cloned into BamHI/XhoI sites of pCDNA4a (Invitrogen) to produce MycHis$_6$ tagged SOD1 construct for mammalian expression. Full-length SOD1 (A4V), cDNA (within pBCM vector) underwent site-directed mutagenesis (Roche) to make additional point mutations. SOD1 mRNA was synthesised *in vitro* using a mMESSAGE mMACHINE T3 Promoter Kit (Ambion). His-tagged SOD1 construct for expression in *E. coli* was made by subcloning of SOD1 into BamHI/XhoI sites of or modified pET30a plasmid (Merck biosciences), in which TEV protease cleavage site (ENLYFQ/G) was inserted between the N-terminal His$_6$ tag and the SOD1 sequence. To make pET30a-Hsp70, Hsp70 was subcloned from pcDNA5/FRT/TO-HSPA1A plasmid, which was a gift from Harm Kampinga (Addgene plasmid #19456) (Hageman and Kampinga, 2009), into pET30a.

Protein purification

For peptide affinity studies, the His-tagged recombinant Hsp70 was purified using conventional Ni-affinity purification protocol (Qiagen). Briefly, protein was overexpressed in C41 (DE3) cells overnight at 25°C in TB medium after induction with 1 mM IPTG. Cells were lysed by high-pressure cell cracker in lysis buffer (TBS containing 15 mM imidazole), and supernatant was cleared by centrifugation at 12 000 rpm for 20 min. Supernatant was incubated with Ni-agarose for 30 min, followed by washes with 200 volumes of lysis buffer, and protein was eluted in TBS containing 250 mM imidazole. In a second step, protein was purified by size-exclusion chromatography on Superdex G-75 columns in TBS buffer and concentrated using Centricon units (Millipore).

Cell culture and transfections

The human cervix adenocarcinoma cell line HeLa and the mouse motor neuron-like hybrid cell line NSC-34 were cultured according to standard procedures in Dulbecco's Modified Eagle Medium supplemented with 10% FBS, 1 mM sodium pyruvate and non-essential amino acids. All cell culture media and supplements were obtained from Gibco/ThermoFisher.

Cells were transfected using the Fugene HD (Promega) transfection reagent according to the manufacturer's protocol. Stable SOD-1 expressing NSC-34 cell lines were generated by selection with Zeocin (Gibco—ThermoFisher).

Immunofluorescence

HeLa cells were plated (3×10^4) and transfected on glass 8-well chamber slides. Twenty-four hours after transfection, the cells were fixed with 4% formaldehyde (5 min, RT), washed in Tris Buffer Saline pH 7.4 (TBS), permeabilized in 0.2% Triton X-100 in TBS (5 min, RT) and blocked (2×15 mins, RT) in a blocking buffer (5% BSA in TBS). The primary antibodies, mouse anti-myc tag (ThermoFisher; 1/1000) and rat anti-Hsp70 (Cell Signalling; 1/1000) were diluted in blocking buffer and incubated 1 hr at RT. The secondary antibodies (goat anti-mouse Alexa Fluor 594 and goat anti-rat Alexa Fluor 488) were diluted 1:1000 and incubated for 1 h at RT. The slides were mounted with ProLong Gold Antifade Reagent containing DAPI (ThermoFisher). Images were acquired using a Leica SP8x confocal microscope.

Solubility fractionation

Twenty-four hours after transfection, HeLa cells were lysed in NP40 buffer (150 mM NaCl, 50 mM Tris HCl pH 8, 1% IGEPAL(NP40), ×1 complete inhibitor (Roche), 1 U/µl Universal Nuclease (Pierce)). Extracts were kept on ice for 45 min after which the insoluble fraction was collected by centrifugation for 10 min at 17×10^3 rcf at 4°C. The supernatant was collected as the NP40 soluble fraction, while the pellet was redissolved in 8 M Urea. Protein extracts were fractionated by SDS-PAGE and analysed by western blot (see below).

Filter trapping

Transfected cells were lysed at indicated time points in a RIPA buffer. Whole, non-cleared lysates were next filtered through Spin-X 0,22 µm cellulose acetate filters by centrifugation at 17×10^3 rcf for 15 min. Proteins trapped on the filter were extracted by a serial approach: (i) first, filters were incubated in RIPA buffer containing 2% SDS at 95°C for 10 min, followed by a centrifugation step as before; and (ii) next, the filters were incubated in 8 M Urea for 30 min at RT and centrifuged again. Different fractions were fractionated and quantified as described above.

Immunoprecipitations

For co-immunoprecipitations, HeLa cells were transfected in six-well plates. Twenty-four hours after transfection, cells were lysed in NP40 buffer (see above) supplemented with 1 U/µl hexokinase (Sigma) and 10 mM D-glucose (Sigma). Lysates were incubated with a mouse anti-myc antibody (1/100, ThermoFisher) overnight at 4°C on a rotor. In parallel, magnetic beads (Dynabeads, Invitrogen) were blocked in 5% BSA/TBS. Next day, the antibodies in lysates were trapped on the magnetic beads, and washed extensively in NP40 buffer. Bound proteins were dissociated from the antibodies by boiling the magnetic beads in ×1 western blot sample buffer.

In vitro peptide binding

In order to make overlapping library covering entire SOD1 sequence, 7-mer peptides where chemically sensitised on cellulose ß-alanine membranes with a *t* residue window (PepSpot membranes, JPT Peptide Technologies, GmbH). Prior to incubation, the membranes were washed in 100% MeOH for 10 min, and three times for 20 min in TBS (20 mM Tris buffer pH 7.5 plus 150 mM NaCl). Following blocking with BSA 2% w/v in TBS for 1 h, the membranes were incubated with 100 nM Hsp70 (Enzo Life Sciences) in MP-buffer (31 mM Tris pH 7.5, 170 mM NaCl, 6.4 mM KCl, 5% Sucrose, 0.05% Tween-20) for 1 h. Subsequently membranes were washed three times for 10 min in TBS buffer and incubated for 1 h with mouse monoclonal anti-Hsp70 antibody (clone 8E2/2, Alexis Biosciences) diluted 1:2000 in blocking buffer plus 0.05% v/v Tween20. Membranes were washed three times for 10 min in TBST (TBS buffer plus 0.05% v/v Tween20) and incubated for 30 min with anti-mouse HRP-conjugated antibody (Promega) diluted 1:10000 in blocking buffer plus 0.05% v/v Tween20. The membranes were finally washed two times for 10 min in TBS buffer plus 0.05% Tween20, one time for 10 min in TBS buffer and subjected to chemiluminescent reaction using SuperSignal West Dura substrate (Pierce), detected by CCD camera connected to the ChemiDoc XRS image acquire and process system (BioRad).

Microscale thermophoresis

MST measurements were performed in a Monolith NT.Automated (NanoTemper Technology, München, Germany), in order to determine the binding capacity of the H_{63}FNPLSR$_{69}$ and I_{113}GRTLVV$_{119}$ peptides to Hsc70. Purified Hsc70 was labelled with NT-647 dye through N-hydroxysuccinimide ester (NHS) coupling, following the Nanotemper labelling kit protocol. For MST experiments, NT-647-labelled Hsc70 concentration remained constant (5 nM) in MST buffer (30 mM HEPES, pH 7.0, 150 mM KCl, 5 mM $MgCl_2$, 0.05% Tween20). Peptide stocks were dissolved in DMSO and titrated between 5 mM and 660 nM in MST buffer. After 1 h of incubation at room temperature, samples were loaded in premium-coated glass capillaries and MST measurements were performed in a final content of 5% DMSO. Laser power was set to 10% at 25°C and data analysis was performed using NanoTemper Analysis software v2.1.5.

BN-PAGE and western and dot blots

To make fresh lysates, cells were rinsed with PBS following growth for 24 h after transfection and lysed with NP40 lysis buffer containing Complete protease inhibitor cocktail (Roche). Lysates were fractionated on a 3–12% gradient BN-PAGE gels (ThermoFisher) according to manufacturer's protocol and transferred to a PVDF membrane (Biorad). Membranes were fixed with 8% acetic acid for 10 min, destained with 100% methanol for 10 min and blocked with 5% BSA-TBS-T for 1 h. For western blots, lysates were fractionated on Any kD mini-PROTEAN gels (Biorad), followed by transfer on nitrocellulose membranes (Biorad) and blocking with 5% milk-TBST for 1 h. For detection, membranes were probed with anti-Myc (ThermoFisher), anti-Hsp70, anti-Hsp70B' (Enzo Lifesciences), and anti-GADPH (Santa Cruz) antibodies overnight at 4°C followed by three washes in TBST for 5 min and incubation with the secondary HRP-conjugated antibody (Promega) for 1 h. Following three washes with TBST, the HRP signal was visualised with ECL substrate kit (Millipore) and imaged on a Chemidoc system (Biorad).

Inhibition of protein synthesis.

Protein stability was assayed by blocking protein synthesis in live cells with cycloheximide. Hela cells were transfected with SOD1 plasmids, incubated for 24 h, and 50 µg/ml of cycloheximide was added to the media, followed by incubation for 0, 3, 6 or 9 h after addition of the cycloheximide. Cells were lysed and protein levels were analysed by western blot as described in previous section. Degradation rate was determined by quantifying the ratio of signal for His_6Myc-SOD1 to GAPDH for each timepoint.

Transmission electron microscopy

The peptides were synthesised by solid-phase peptide synthesis at JPT and dissolved in PBS. Samples were imaged after incubation for 2 weeks at room temperature. Aliquots (5 µl) of a peptide preparation was adsorbed to carbon-coated FormVar film on 400-mesh copper grids (Plano GmbH, Germany) for 1 min. The grids were blotted, washed twice in 50 µl droplets of Milli-Q water, and stained with 1% (wt/vol) uranylacetate. Samples were studied with a FEI Morgagni^{TM} 268(D) microscope at 120 kV and a JEOL JEM-2100 microscope at 200 kV.

Zebrafish experiments

All zebrafish experiments were performed in accordance with the guidelines of the Ethical Committee for Animal Experimentation, K.U. Leuven (project approval number P021/2010). 1–4 cell stage zebrafish embryos (AB strain) were microinjected with 2.14 nl of SOD1 mRNA using a FemtoJet injection setup. Embryos were then stored in E3 solution (5 mM NaCl, 0.17 mM KCl, 0.33 mM CaCl2 and 0.33 mM MgSO4 and 0.1% Methylene Blue) at 27.5–28.5°C.

At 30 h post-fertilisation (hpf), morphologically normal zebrafish embryos were fixed in 4% paraformaldehyde in PBS and immunostained to visualise motor neurons (anti-SV2, Developmental Studies Hybridoma Bank). Observers blind to injection group measured the axonal length of the first five ventral motor axons after the yolk sac in each embryo using Lucia software (version 4.9), the average of these five lengths was calculated for each embryo.

To examine the SOD1 protein expression levels in the zebrafish, embryos were dechorionated at 24–28 hpf and transferred to a solution of E3 solution containing 1 mM PMSF. The yolksac of the embryo was removed by suction through a narrow glass pipette three times. Deyolked embryos were transferred to Eppendorf tubes and hand homogenised in T-PER lysis buffer (Peirce) with protease inhibitor added (Complete, Roche). The level of protein expression was measured by western blot analysis as described above for the cell culture lysates, with use of a polyclonal antibody against human SOD1 (Santa Cruz).

Statistical analysis

The data sets for subcellular localization, western blots quantifications and axonal length qPCR were analysed using one-way ANOVA and Dunnett's multiple comparisons test, and the differences were considered significant if $P < 0.05$. The statistical analysis was performed using the GraphPad PRISM software.

Supplementary data

Supplementary data are available at *PEDS* online.

Acknowledgements

The Switch Laboratory was supported by grants from the European Research Council under the European Union's Horizon 2020 Framework Programme ERC Grant agreement 647458 (MANGO) to J.S., the Flanders Institute for Biotechnology (VIB), the University of Leuven ('Industrieel Onderzoeksfonds'), the Funds for Scientific Research Flanders (FWO), the Flanders Agency for innovation by Science and Technology (IWT, SBO Grant 60839) and the Federal Office for Scientific Affairs of Belgium (Belspo), IUAP, Grant Number P7/16.

References

Abel, O., Powell, J.F., Andersen, P.M. and Al-Chalabi, A. (2012) *Hum. Mutat.*, **33**, 1345–1351.

Andersen,P.M. and Al-Chalabi,A. (2011) *Nat. Rev. Neurol.*, **7**, 603–615.

Balch, W.E., Morimoto, R.I., Dillin, A. and Kelly, J.W. (2008) *Science*, **319**, 916–919.

Batulan, Z., Shinder, G.A., Minotti, S., He, B.P., Doroudchi, M.M., Nalbantoglu, J., Strong, M.J. and Durham, H.D. (2003) *J. Neurosci.*, **23**, 5789–5798.

Bence, N.F., Sampat, R.M. and Kopito, R.R. (2001) *Science*, **292**, 1552–1555.

Benilova, I., Karran, E. and De Strooper, B. (2012) *Nat. Neurosci.*, **15**, 349–357.

Bieschke, J., Herbst, M., Wiglenda, T. *et al.* (2012) *Nat. Chem. Biol.*, **8**, 93–101.

Boeckmann, B., Bairoch, A., Apweiler, R. *et al.* (2003) *Nucleic Acids Res.*, **31**, 365–370.

Boillee, S., Yamanaka, K., Lobsiger, C.S., Copeland, N.G., Jenkins, N.A., Kassiotis, G., Kollias, G. and Cleveland, D.W. (2006) *Science*, **312**, 1389–1392.

Brotherton, T.E., Li, Y. and Glass, J.D. (2013) *Neurobiol. Dis.*, **49**, 49–56.

Bucciantini, M., Giannoni, E., Chiti, F., Baroni, F., Formigli, L., Zurdo, J., Taddei, N., Ramponi, G., Dobson, C.M. and Stefani, M. (2002) *Nature*, **416**, 507–511.

Calamai, M., Chiti, F. and Dobson, C.M. (2005) *Biophys. J.*, **89**, 4201–4210.

Campioni, S., Mannini, B., Zampagni, M. *et al.* (2010) *Nat. Chem. Biol.*, **6**, 140–147.

Chattopadhyay, M., Durazo, A., Sohn, S.H., Strong, C.D., Gralla, E.B., Whitelegge, J.P. and Valentine, J.S. (2008) *Proc. Natl. Acad. Sci. USA.*, **105**, 18663–18668.

Chiti, F. and Dobson, C.M. (2006) *Annu. Rev. Biochem.*, **75**, 333–366.

Ciechanover, A. and Kwon, Y.T. (2015) *Exp. Mol. Med.*, **47**, e147.

Cohen, E., Bieschke, J., Perciavalle, R.M., Kelly, J.W. and Dillin, A. (2006) *Science*, **313**, 1604–1610.

Dal Canto, M.C. (1995) *Clin. Neurosci.*, **3**, 332–337.

Dobson, C.M. (2006) *Protein Pept. Lett.*, **13**, 219–227.

Fandrich, M. (2012) *J. Mol. Biol.*, **421**, 427–440.

Fernandez-Escamilla, A.M., Rousseau, F., Schymkowitz, J. and Serrano, L. (2004) *Nat. Biotechnol.*, **22**, 1302–1306.

Flechtner, J.B., Cohane, K.P., Mehta, S., Slusarewicz, P., Leonard, A.K., Barber, B.H., Levey, D.L. and Andjelic, S. (2006) *J. Immunol.*, **177**, 1017–1027.

Gidalevitz, T., Ben-Zvi, A., Ho, K.H., Brignull, H.R. and Morimoto, R.I. (2006) *Science*, **311**, 1471–1474.

Grossmann, M.E., Madden, B.J., Gao, F., Pang, Y.P., Carpenter, J.E., McCormick, D. and Young, C.Y. (2004) *Exp. Cell Res.*, **297**, 108–117.

Guo, Y., Li, C., Wu, D., Wu, S., Yang, C., Liu, Y., Wu, H. and Li, Z. (2010) *Brain Res.*, **1353**, 234–244.

Hageman, J. and Kampinga, H.H. (2009) *Cell Stress Chaperones*, **14**, 1–21.

Hardy, J. and Selkoe, D.J. (2002) *Science*, **297**, 353–356.

Ivanova, M.I., Sievers, S.A., Guenther, E.L., Johnson, L.M., Winkler, D.D., Galaleldeen, A., Sawaya, M.R., Hart, P.J. and Eisenberg, D.S. (2014) *Proc. Natl. Acad. Sci. USA.*, **111**, 197–201.

Kaganovich, D., Kopito, R. and Frydman, J. (2008) *Nature*, **454**, 1088–1095.

Khare, S.D., Wilcox, K.C., Gong, P. and Dokholyan, N.V. (2005) *Proteins: Struct. Funct. Bioinf.*, **61**, 617–632.

Krishnan, J., Lemmens, R., Robberecht, W. and Van Den Bosch, L. (2006) *Exp. Neurol.*, **200**, 301–310.

Lang, L., Kurnik, M., Danielsson, J. and Oliveberg, M. (2012) *Proc. Natl. Acad. Sci. USA.*, **109**, 17868–17873.

Lemmens, R., Van Hoecke, A., Hersmus, N., Geelen, V., D'Hollander, I., Thijs, V., Van Den Bosch, L., Carmeliet, P. and Robberecht, W. (2007) *Hum. Mol. Genet.*, **16**, 2359–2365.

Lin, P.Y., Simon, S.M., Koh, W.K., Folorunso, O., Umbaugh, C.S. and Pierce, A. (2013) *Mol Neurodegener*, **8**, 43.

Liu, J., Shinobu, L.A., Ward, C.M., Young, D. and Cleveland, D.W. (2005) *J. Neurochem.*, **93**, 875–882.

Mackenzie, I.R.A., Rademakers, R. and Neumann, M. (2010) *Lancet Neurol.*, **9**, 995–1007.

Maurer-Stroh, S., Debulpaep, M., Kuemmerer, N. *et al.* (2010) *Nat. Methods*, **7**, 237–U109.

Mendillo, M.L., Santagata, S., Koeva, M., Bell, G.W., Hu, R., Tamimi, R.M., Fraenkel, E., Ince, T.A., Whitesell, L. and Lindquist, S. (2012) *Cell*, **150**, 549–562.

Nagai, M., Aoki, M., Miyoshi, I., Kato, M., Pasinelli, P., Kasai, N., Brown, R.H.Jr. and Itoyama, Y. (2001) *J. Neurosci.*, **21**, 9246–9254.

Okochi, M., Hayashi, H., Ito, A., Kato, R., Tamura, Y., Sato, N. and Honda, H. (2008) *J. Biosci. Bioeng.*, **105**, 198–203.

Perrin, R.J., Fagan, A.M. and Holtzman, D.M. (2009) *Nature*, **461**, 916–922.

Polymenidou, M. and Cleveland, D.W. (2011) *Cell*, **147**, 498–508.

Proctor, E.A., Fee, L., Tao, Y. *et al.* (2016) *Proc. Natl. Acad. Sci. USA.*, **113**, 614–619.

Ramesh, T., Lyon, A.N., Pineda, R.H., Wang, C., Janssen, P.M., Canan, B.D., Burghes, A.H. and Beattie, C.E. (2010) *Dis. Model. Mech.*, **3**, 652–662.

Redler, R.L., Fee, L., Fay, J.M., Caplow, M. and Dokholyan, N.V. (2014) *Biochemistry*, **53**, 2423–2432.

Rosen, D.R., Bowling, A.C., Patterson, D. *et al.* (1994) *Hum. Mol. Genet.*, **3**, 981–987.

Rousseau, F., Schymkowitz, J. and Oliveberg, M. (2008) *Proc. Natl. Acad. Sci. USA.*, **105**, 18649–18650.

Rudiger, S., Germeroth, L., SchneiderMergener, J. and Bukau, B. (1997) *EMBO J.*, **16**, 1501–1507.

Sangwan, S., Zhao, A., Adams, K.L. *et al.* (2017) *Proc. Natl. Acad. Sci. USA.*, **114**, 8770–8775.

Schymkowitz, J., Borg, J., Stricher, F., Nys, R., Rousseau, F. and Serrano, L. (2005) *Nucleic Acids Res.*, **33**, W382–W388.

Siekierska, A., De Baets, G., Reumers, J., Gallardo, R., Rudyak, S., Broersen, K., Couceiro, J., Van Durme, J., Schymkowitz, J. and Rousseau, F. (2012) *J. Biol. Chem.*, **287**, 28386–28397.

Silva, M.C., Fox, S., Beam, M., Thakkar, H., Amaral, M.D. and Morimoto, R.I. (2011) *PLoS Genet.*, **7**, e1002438.

Stevens, S.Y., Cai, S., Pellecchia, M. and Zuiderweg, E.R. (2003) *Protein Sci.*, **12**, 2588–2596.

Swain, J.F., Schulz, E.G. and Gierasch, L.M. (2006) *J. Biol. Chem.*, **281**, 1605–1611.

Takeda, S. and McKay, D.B. (1996) *Biochemistry*, **35**, 4636–4644.

Takenaka, I.M., Leung, S.M., McAndrew, S.J., Brown, J.P. and Hightower, L.E. (1995) *J. Biol. Chem.*, **270**, 19839–19844.

Taylor, J.P., Brown, R.H.Jr. and Cleveland, D.W. (2016) *Nature*, **539**, 197–206.

van der Kant, R., Karow-Zwick, A.R., Van Durme, J. *et al.* (2017) *J. Mol. Biol.*, **429**, 1244–1261.

Van Durme, J., Maurer-Stroh, S., Gallardo, R., Wilkinson, H., Rousseau, F. and Schymkowitz, J. (2009) *PLoS Comput. Biol.*, **5**, e1000475.

Van Hoecke, A., Schoonaert, L., Lemmens, R. *et al.* (2012) *Nat. Med.*, **18**, 1418–1422.

Vassall, K.A., Stubbs, H.R., Primmer, H.A. *et al.* (2011) *Proc. Natl. Acad. Sci. USA.*, **108**, 2210–2215.

Ventura, S., Zurdo, J., Narayanan, S. *et al.* (2004) *Proc. Natl. Acad. Sci. USA.*, **101**, 7258–7263.

Vleminckx, V., Van Damme, P., Goffin, K., Delye, H., Van Den Bosch, L. and Robberecht, W. (2002) *J. Neuropathol. Exp. Neurol.*, **61**, 968–974.

Walker, L.C. and LeVine, H.3rd (2012) *J. Biol. Chem.*, **287**, 33109–33115.

Wang, G. and Fersht, A.R. (2017) *Proc. Natl. Acad. Sci. USA.*, **114**, E2634–E2643.

Wang, J., Farr, G.W., Hall, D.H., Li, F., Furtak, K., Dreier, L. and Horwich, A.L. (2009) *PLoS Genet.*, **5**, e1000350.

Watanabe, M., Dykes-Hoberg, M., Culotta, V.C., Price, D.L., Wong, P.C. and Rothstein, J.D. (2001) *Neurobiol. Dis.*, **8**, 933–941.

Wijesekera, L.C. and Leigh, P.N. (2009) *Orphanet J. Rare Dis.*, **4**, 3.

Winklhofer, K.F., Tatzelt, J. and Haass, C. (2008) *EMBO J.*, **27**, 336–349.

Wood, H. (2011) *Nat. Rev. Neurol.*, **7**.

Xu, J., Reumers, J., Couceiro, J.R. *et al.* (2011) *Nat. Chem. Biol.*, **7**, 285–295.

Zetterstrom, P., Stewart, H.G., Bergemalm, D., Jonsson, P.A., Graffmo, K.S., Andersen, P.M., Brannstrom, T., Oliveberg, M. and Marklund, S.L. (2007) *Proc. Natl. Acad. Sci. USA.*, **104**, 14157–14162.